

# Mechanically patterned neuromuscular junctions-in-a-dish have improved functional maturation

Cassandra L. Happe<sup>a</sup>, Kevin P. Tenerelli<sup>a</sup>, Anastasia K. Gromova<sup>b</sup>, Frederic Kolb<sup>a,†</sup>,  
and Adam J. Engler<sup>a,b,c,\*</sup>

<sup>a</sup>Department of Bioengineering and <sup>b</sup>Biomedical Sciences Program, University of California, San Diego, La Jolla, CA 92093; <sup>c</sup>Sanford Consortium for Regenerative Medicine, La Jolla, CA 92037

**ABSTRACT** Motor neuron (MN) diseases are progressive disorders resulting from degeneration of neuromuscular junctions (NMJs), which form the connection between MNs and muscle fibers. NMJ-in-a-dish models have been developed to examine human MN-associated dysfunction with disease; however such coculture models have randomly oriented myotubes with immature synapses that contract asynchronously. Mechanically patterned (MP) extracellular matrix with alternating soft and stiff stripes improves current NMJ-in-a-dish models by inducing both mouse and human myoblast durotaxis to stripes where they aligned, differentiated, and fused into patterned myotubes. Compared to conventional culture on rigid substrates or unpatterned hydrogels, MP substrates supported increased differentiation and fusion, significantly larger acetylcholine (ACh) receptor clusters, and increased expression of MuSK and Lrp4, two cell surface receptors required for NMJ formation. Robust contractions were observed when mouse myotubes were stimulated by ACh, with twitch duration and frequency most closely resembling those for mature muscle on MP substrates. Fused myotubes, when cocultured with MNs, were able to form even larger NMJs. Thus MP matrices produce more functionally active NMJs-in-a-dish, which could be used to elucidate disease pathology and facilitate drug discovery.

**Monitoring Editor**  
Alex Dunn  
Stanford University

Received: Jan 19, 2017  
Revised: Apr 3, 2017  
Accepted: May 2, 2017

## INTRODUCTION

Neuromuscular junctions (NMJs) are specialized synapses that form between motor neurons (MNs) and skeletal muscle fibers. On activation, presynaptic MNs release acetylcholine (ACh) into the synaptic cleft, which then binds to ACh receptors (AChRs) present on the postsynaptic muscle membrane; AChR ligation induces muscle fiber

contraction. Diseases affecting MNs, such as amyotrophic lateral sclerosis (ALS), are characterized by the loss of NMJs as MNs degenerate during disease progression (Wijesekera and Leigh, 2009; Viollet and Melki, 2013). This class of diseases is particularly debilitating, as MN loss leads to muscle atrophy and paralysis and is often fatal. With limited treatment options that only extend lifespan by months (Engler *et al.*, 2004), significant efforts have focused on refining *in vivo* disease models to test new therapeutic options. However, current animal models for many MN diseases replicate only a portion of the spectrum of phenotypes in human disease (Pioro and Mitsumoto, 1995; Picher-Martel *et al.*, 2016).

Coculture systems to create NMJs *in vitro* were developed to address concerns about animal models (Das *et al.*, 2007, 2010). More recent versions use stem cell-derived MNs and cell line-derived (Umbach *et al.*, 2012; Morimoto *et al.*, 2013; Uzel *et al.*, 2016), primary cell-derived (Chipman *et al.*, 2014; Steinbeck *et al.*, 2016), or stem cell-derived muscle (Demestre *et al.*, 2015; Puttonen *et al.*, 2015). Using human induced pluripotent stem cells in such systems has further enabled patient-specific MN disease modeling (Faravelli *et al.*, 2014; Abujarour and Valamehr, 2015; Lenzi *et al.*, 2016) and drug screening (Inoue *et al.*, 2014). Although having human cells enables more complex NMJ-in-a-dish modeling, concerns about

This article was published online ahead of print in MBoC in Press (<http://www.molbiolcell.org/cgi/doi/10.1091/mbc.E17-01-0046>) on May 11, 2017.

<sup>†</sup>Present address: Institut Gustave Roussy, 94800 Villejuif, France.

\*Address correspondence to: Adam J. Engler (aengler@ucsd.edu).

Abbreviations used: ACh, acetylcholine; AChR, acetylcholine receptor; AFM, atomic force microscopy; ALS, amyotrophic lateral sclerosis; BTX, bungrotoxin; 2D, two-dimensional; 3D, three-dimensional; ECM, extracellular matrix; FBS, fetal bovine serum; GAPDH, glyceraldehyde-3-phosphate dehydrogenase; hESC, human embryonic stem cell; Lrp4, low-density lipoprotein receptor-related protein 4; MN, motor neuron; MP, mechanically patterned; MuSK, muscle-specific kinase; NMJ, neuromuscular junction; PA, polyacrylamide; PBS, phosphate-buffered saline; Sulfo-SANPAH, sulfosuccinimidyl 6-(4'-azido-2'-nitrophenylamino)hexanoate; UV, ultraviolet;  $\mu$ CP, microcontact printing.

© 2017 Happe *et al.* This article is distributed by The American Society for Cell Biology under license from the author(s). Two months after publication it is available to the public under an Attribution–Noncommercial–Share Alike 3.0 Unported Creative Commons License (<http://creativecommons.org/licenses/by-nc-sa/3.0>).

"ASCB," "The American Society for Cell Biology," and "Molecular Biology of the Cell" are registered trademarks of The American Society for Cell Biology.

MN, skeletal muscle, and NMJ maturity have been raised (Siller *et al.*, 2013). Moreover, NMJ development relies on the organization of embryonic muscle fibers, precise guidance of MN axons, and the interplay of signaling from both the presynaptic and postsynaptic cells (Witzemann, 2006; Wu *et al.*, 2010; Singhal and Martin, 2011; Shi *et al.*, 2012). Traditional unpatterned *in vitro* coculture models on rigid substrates do not faithfully recapitulate the complex architecture observed *in vivo*; myotubes exhibit poor fusion efficiency and are highly disorganized, leading to inefficient and irregular contraction (Das *et al.*, 2007, 2010; Guo *et al.*, 2011; Umbach *et al.*, 2012). Unpatterned NMJ cultures also do not develop sufficiently large AChR clusters—postsynaptic membrane specializations that are a hallmark of functional, mature NMJs (Witzemann, 2006).

To improve cell and NMJ maturation in coculture systems, some studies used microcontact printing ( $\mu$ CP), topography, and three-dimensional (3D) molds to organize myotubes *in vitro*.  $\mu$ CP guides cell growth by constraining cells to areas where extracellular matrix (ECM) proteins have been selectively deposited (Chen *et al.*, 1997). Myoblasts attach and fuse on patterned ECM, creating aligned myotubes (Engler *et al.*, 2004; Altomare *et al.*, 2010). Over time, however, proteins from culture medium may deposit on the substrate, obscure the pattern, and eliminate cell alignment (Choi *et al.*, 2012b). Physical stimuli, including topographical cues, have also been used to align myotubes *in vitro* (Wang *et al.*, 2012), but these systems use substrates orders of magnitude more rigid than muscle (Choi *et al.*, 2012a). They often result in muscle that is thinner and less mature than their *in vivo* counterparts (Gaudel *et al.*, 2008; Zhu *et al.*, 2011; Lawlor *et al.*, 2014; Gibbons *et al.*, 2016). Both of these approaches rely on two-dimensional (2D) methods, so 3D models have been developed that create aligned myobundles, which persist for several

weeks in culture. Generally, these constructs are produced by using micromolds in which myoblasts are cultured (Morimoto *et al.*, 2013; Madden *et al.*, 2015; Bettadapur *et al.*, 2016) or via self-assembly around T-shaped flexible posts (Sakar *et al.*, 2012; Cvetkovic *et al.*, 2014; Raman *et al.*, 2016); however, both are often fabricated with complicated lithography processes, and resultant systems are difficult to process and image based on their 3D structure.

Methods that produce mature muscle but also rely on simple fabrication methods could be optimal for widespread use in NMJ-in-a-dish models. In this article, we describe a simple mechanically patterned hydrogel that can be used as a MN and myotube coculture platform. The system is based on a micropatterned hydrogel cell culture substrate that aligns cultured myotubes by juxtaposing soft and stiff regions similar to the alternating pattern of aligned myotubes with adjacent softer neurons to innervate the firm muscle *in vivo* (Choi *et al.*, 2012b). Such patterns result in improved fusion, differentiation, and AChR formation for cells of either mouse or human origin that are responsive to pharmacological stimuli and, on coculture with MNs, form functional NMJs, thus providing a significant improvement over standard cell culture vessels without the requirement of expensive specialized equipment.

## RESULTS

### Design and fabrication of mechanically patterned hydrogels

We developed a two-step photopolymerization method that produces polyacrylamide (PA) hydrogels containing a grating pattern with alternating elasticity profiles (Figure 1A), resulting in a hydrogel with 100- $\mu$ m-wide “stiff” stripes interspersed with 200- $\mu$ m-wide “soft” stripes, that is, alternating regions of  $12.6 \pm 0.63$  and  $0.72 \pm 0.05$  kPa, respectively, as measured by atomic force microscopy (Figure 1B). Using this method, we successfully fabricated a wide range of geometrical patterns with micrometer-sized features. A sharp change in stiffness was observed at the interface of soft and stiff regions, creating a steep gradient of  $>100$  kPa/mm, consistent with prior observation (Vincent *et al.*, 2013) and indicating that there was limited diffusion during photopolymerization. For this NMJ-in-a-dish system, we chose to model myogenic and neurogenic stiffness (Engler *et al.*, 2006), although elastic properties can be easily modified by changing acrylamide concentrations and micropattern dimensions for alternate applications.

### Improved myotube fusion and differentiation on mechanically patterned hydrogels

Mouse C2C12 and human embryonic stem cell (hESC)-derived myoblasts (Caron *et al.*, 2016) were cultured on mechanically patterned hydrogels to assess the influence of mechanical patterning on myotube fusion and differentiation. To decouple the effect of the compliant hydrogel from the mechanical patterning, myoblasts were also cultured on an unpatterned, myogenic hydrogel and on glass. Within 24 h, myoblasts preferentially migrated to and aligned with the

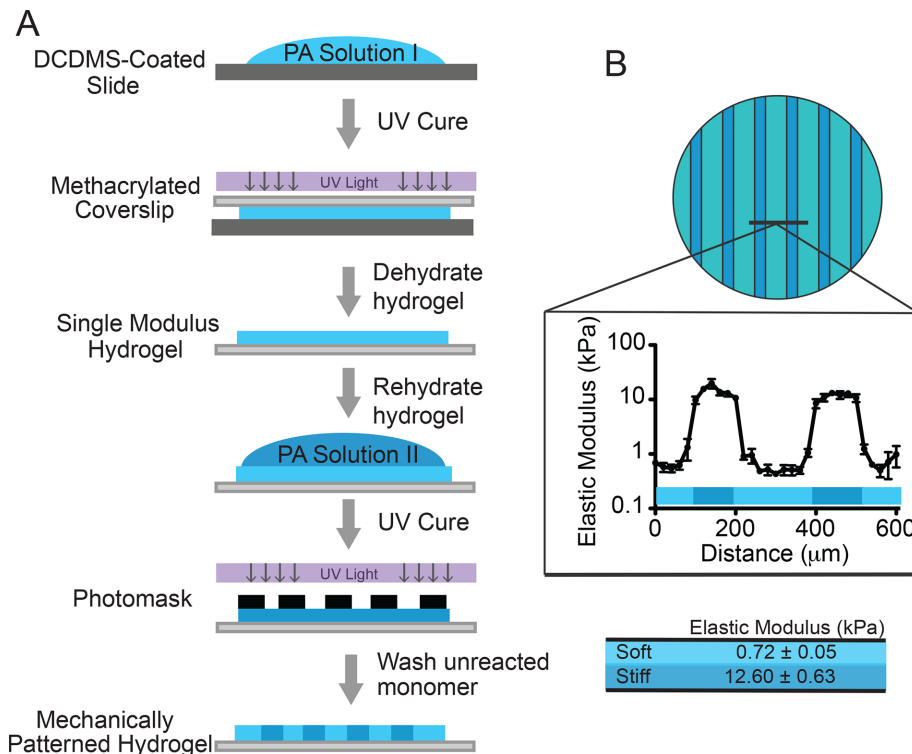


**FIGURE 1:** Fabrication of mechanically patterned hydrogel. (A) Patterning process by which sequential exposures of the hydrogel to UV light—the second exposure including a photomask—creates the patterned hydrogel. (B) Hydrogel pattern and plot of elastic modulus vs. position orthogonal to the pattern direction. Average modulus values for “soft” (teal) and “stiff” (blue) regions.

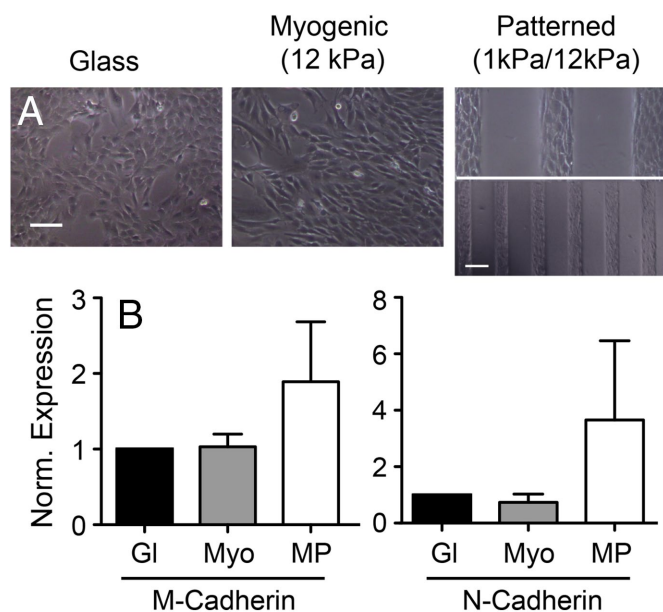


**FIGURE 2:** Durotactic pattern recognition and fusion marker expression. (A) Bright-field images of mouse myoblasts on the indicated substrates. Scale bar, 100  $\mu$ m. Inset, low-magnification bright-field image of mouse myoblasts on the mechanically patterned substrate. Scale bar, 200  $\mu$ m. (B) mRNA transcript levels for M-cadherin (left) and N-cadherin (right) for the indicated conditions. Data were normalized to glass substrates ( $n = 5$ ).

stiffer myogenic regions on the mechanically patterned hydrogel, whereas myoblasts on the unpatterned hydrogels and glass exhibited no organization (Figure 2A), consistent with myocytes and stem cells (Choi *et al.*, 2012b; Vincent *et al.*, 2013; Wen *et al.*, 2015). Before differentiation, myoblasts on patterned hydrogels also expressed more mRNA of M- and N-cadherin, markers indicative of cell fusion (Figure 2B).

After myogenic differentiation was initiated, elongated and multinucleated myotubes were present on all three substrates. However, the fusion index and average myotube width were larger on the mechanically patterned substrates than for both the unpatterned myogenic hydrogel and glass (Figure 3, A–C); only myotubes on patterned hydrogels approach sizes consistent with *in vivo* muscle, independent of species (Gaudel *et al.*, 2008; Zhu *et al.*, 2011; Lawlor *et al.*, 2014; Gibbons *et al.*, 2016). In addition to fusion indices, mouse myoblasts expressed MyoD and myogenin transcription factors on mechanically patterned hydrogels in a temporally regulated manner (Figure 3D), consistent with their sequential expression during differentiation (Choi *et al.*, 2012a). Mechanically patterned human myotubes also expressed significantly more myosin heavy chain transcript, whereas mouse myotubes tended toward higher expression, suggesting that they are more mature than myotubes cultured on unpatterned myogenic hydrogels or glass (Figure 3, E and F). Together these data suggest that alignment, in addition to substrate elastic properties, could drive maturation and fusion, which may also contribute to deficiencies previously observed in hESC-derived myotube fusion (Demestre *et al.*, 2015; Puttonen *et al.*, 2015).

### Mechanical patterning drives formation of functional AChR clusters

AChRs are critical components of NMJs and must be clustered in fused myotubes to function (Huh and Fuhrer, 2002). MNs secrete

agrin to induce clustering, and so, on addition of exogenous agrin, we determined whether mechanical patterning could enhance AChR clustering. For both humans and mice, we found the largest AChR cluster sizes in myotubes cultured on mechanically patterned hydrogels (Figure 4, A and B). During NMJ development, agrin is released from approaching MNs and binds a receptor complex on the myotube consisting of dimers of muscle-specific receptor tyrosine kinase (MuSK) and low-density lipoprotein receptor-associated protein (Lrp4), initiating a signaling cascade that induces AChR clustering (Figure 4C; Wu *et al.*, 2010; Shi *et al.*, 2012). Lrp4 transcript was most highly expressed in myotubes in mechanically patterned myotubes, independent of species (Figure 4D). MuSK transcript was similarly highest with mechanically patterned hydrogels, but only in human myotubes (Figure 4E). To determine whether endogenous agrin from MN coculture could drive cluster formation, we cocultured primary MNs after myoblast fusion into myotubes. Cocultures were initiated after 4 d of myotube differentiation and maintained for 7 d. We found that mechanically patterned hydrogels drove formation of the largest AChR clusters, whereas AChR clusters on both the glass and unpatterned myogenic substrates remained small and punctate (Figure 5, A and B). In the coculture system, MNs generally reside on top of the existing regions of mechanically patterned myotubes, avoiding the softer areas, and extend neurite outgrowths that terminate on the myotubes, with some instances of colocalization with AChR clusters, an indicator of putative NMJ formation (Figure 5C). Together these data suggest that NMJ-in-a-dish systems should support robust myotube alignment to facilitate AChR clustering, but these data do not yet establish the propagation of signals across the forming NMJ.

Spontaneous contractions were observed for myotube cultures only with mechanically patterned hydrogels (Figure 6, A and B, left); spontaneous activity increases during development, and thus our data are consistent with mechanically patterned myotubes being more functionally mature than unpatterned myotubes (Altomare *et al.*, 2010). Although these data suggest functional clusters in the NMJ-in-a-dish system, they do not establish that the junctions are indeed functional. To determine whether AChR clusters can stimulate contraction, we exogenously added a bolus of 1 mM ACh. On stimulation, myotubes on both glass and mechanically patterned hydrogels contracted, although mechanically patterned myotubes underwent larger displacements during contraction, indicating a more intense contraction (Figure 6, A and B, right). Mechanically patterned myotube contractions were also shorter in duration and occurred at a higher frequency than myotube contractions on glass (Figure 6, C and D), again suggesting that the AChR clusters, which are a critical component of NMJs, are more functionally mature.

### Substrate compliancy mediates clustering of ACh receptors on mechanically patterned hydrogels

To examine the roles of culture substrate stiffness versus myotube fusion and assembly in AChR clustering during NMJ development on mechanically patterned hydrogels, we cultured mouse myoblasts on patterned hydrogels with pathological stiff regions (Figure 7). After denervation—a hallmark of MN diseases—muscle fiber atrophy is accompanied by increased fibrosis, which increases the elastic modulus of muscle tissue (Engler *et al.*, 2004; Carlson, 2014). Thus we fabricated mechanically patterned hydrogels with alternating soft (0.8 kPa) and pathological (58.1 kPa) stripes (Figure 7A). Mouse myoblasts differentiated on the pathological patterns showed no difference in fusion or myotube width from those cultured on patterned substrates with myogenic stiff regions (Figure 7, B and C). AChR cluster area was sensitive to elastic modulus, with myotubes cultured on the pathological patterns expressing smaller

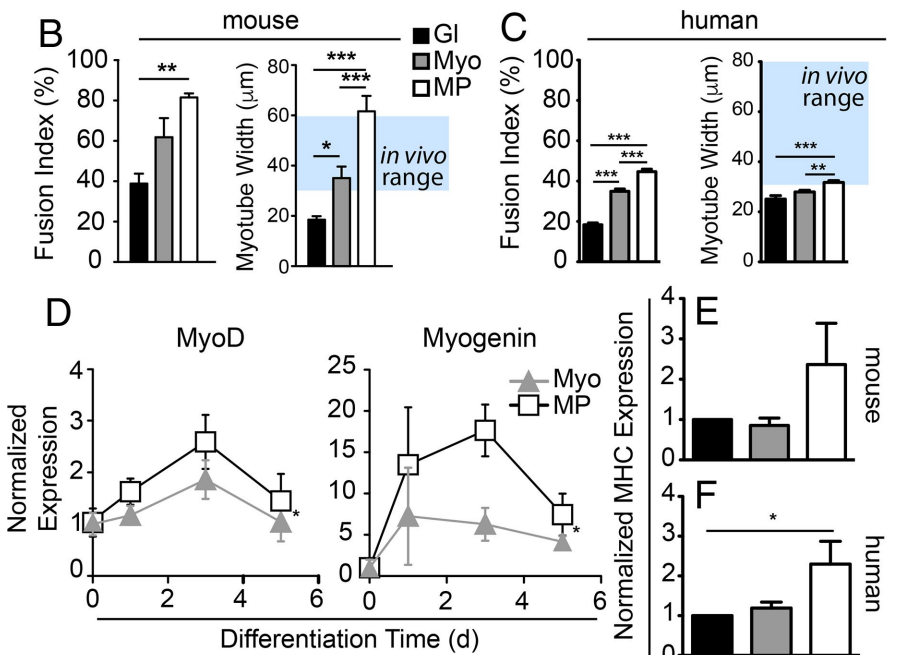
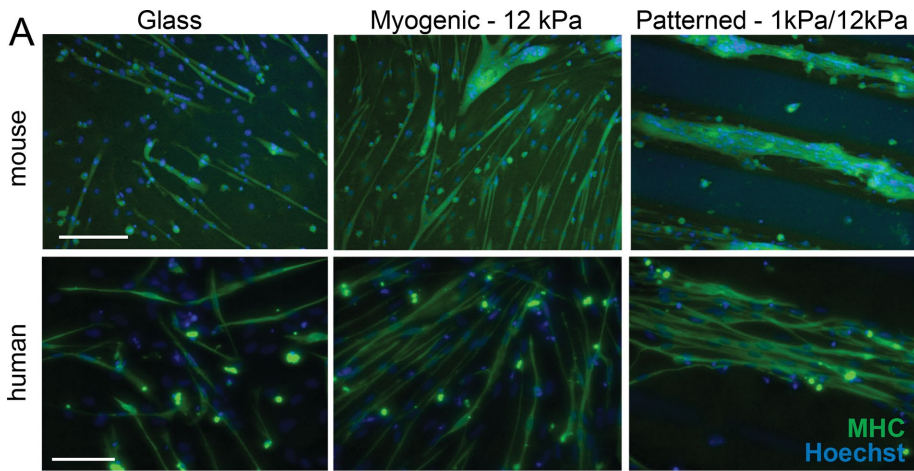


**FIGURE 3:** Improved myoblast fusion and differentiation on mechanically patterned matrices. (A) Representative fluorescence images of myotubes cultured on glass, myogenic (Myo), or mechanically patterned (MP) hydrogels at 5 d (mouse) or 7 d (human) after induction of differentiation. Cells were immunolabeled for myosin heavy chain (MHC, green) and counterstained for nuclei with Hoechst 33352 (blue). Scale bars, 30  $\mu\text{m}$ . Fusion index ( $n = 10$ ) and average myotube width ( $n = 30\text{--}88$  individual myotubes per condition) for both (B) mouse and (C) human myotubes. The shaded region denotes the *in vivo* range of myotube width (Gaudel *et al.*, 2008; Zhu *et al.*, 2011; Lawlor *et al.*, 2014; Gibbons *et al.*, 2016). (D) mRNA expression of MyoD and myogenin normalized to day 0 for each condition plotted for the indicated number of days after induction of differentiation ( $n = 6$ ). Data are shown for both substrates of myogenic stiffness, that is, 12 kPa (closed triangles), and with a mechanical pattern (open squares); expression levels are time dependent ( $p < 0.05$ ). (E, F) MHC was assessed by qPCR, and data were normalized to GAPDH and plotted for glass, myogenic substrates, and mechanically patterned hydrogels ( $n = 5$ ). \* $p < 0.05$ , \*\* $p < 0.01$ , and \*\*\* $p < 0.001$  based on ANOVA comparisons of the indicated groups.

AChR clusters than those cultured on myogenic mechanically patterned substrates (Figure 7, D and E), indicating that a previously unknown mechanotransduction pathway mediates AChR clustering. However, there was no correlation between myotube width and the size of the AChR clusters it expressed (Figure 7F), indicating that the mechanism of AChR clustering is independent of the extent of myotube fusion.

dose of agrin added to the culture medium at day 1 after the onset of differentiation. Myotubes cultured on the mechanically patterned substrate, but not on glass or unpatterned myogenic substrates, express up-regulated levels of Lrp4 transcript (Figure 4D). Lrp4 acts as a receptor for agrin and, through its interactions with MuSK, initiates an intracellular cascade that results in AChR clustering on the muscle surface (Kim *et al.*, 2008; Zhang *et al.*, 2008). Thus lower

## DISCUSSION

Despite the proliferation of culture methods to assemble NMJs (Das *et al.*, 2007, 2010; Umbach *et al.*, 2012; Morimoto *et al.*, 2013; Chipman *et al.*, 2014; Faravelli *et al.*, 2014; Inoue *et al.*, 2014; Abujarour and Valamehr, 2015; Demestre *et al.*, 2015; Puttonen *et al.*, 2015; Lenzi *et al.*, 2016; Steinbeck *et al.*, 2016; Uzel *et al.*, 2016) and probe their mechanics (Tay *et al.*, 2016), the possibility of functional neuron-to-muscle connectivity is insufficiently validated due to technical limitations with *in vitro* coculture systems. The mechanically patterned hydrogel system described here creates more mature (and wider) myotubes with larger AChR clusters that are more responsive to ACh than conventional or topographically patterned substrates. This is likely the result of agrin secretion by MN, which signals through MuSK and Lrp4 to induce NMJ assembly (Wu *et al.*, 2010). Forced clustering of myotubes on stiffer stripes also likely drives alignment by overlapping their traction forces, as well as increasing the probability that M- and N-cadherin-rich regions will make contact between cells, a step that is required for fusion (Choi *et al.*, 2012a,b). Alignment of hESC-derived myotubes also illustrates that mechanical patterns may help to specify muscle during development and provides a platform for drug discovery.

During NMJ development, AChR clustering initiated by agrin signaling is a hallmark of the maturing NMJ synapse (Huh and Fuhrer, 2002; Witzemann, 2006). On the mechanically patterned culture system, AChR clustering significantly improves compared with both the glass and unpatterned myogenic culture substrates (Figure 4). In addition, we found that under coculture conditions in which the myotubes are exposed to endogenous agrin released from MNs, mechanically patterned myotubes exhibit AChR clusters that are  $>20\times$  larger than those in myotube monocultures treated with rat recombinant agrin; however, myotubes cultured on glass or unpatterned myogenic substrates do not respond in such a robust manner (Figures 4B and 5B). We attribute the improved clustering to the fact that the MNs likely continuously release agrin onto the myotubes at a physiologically relevant level, whereas in the monoculture, myotubes were exposed to only one

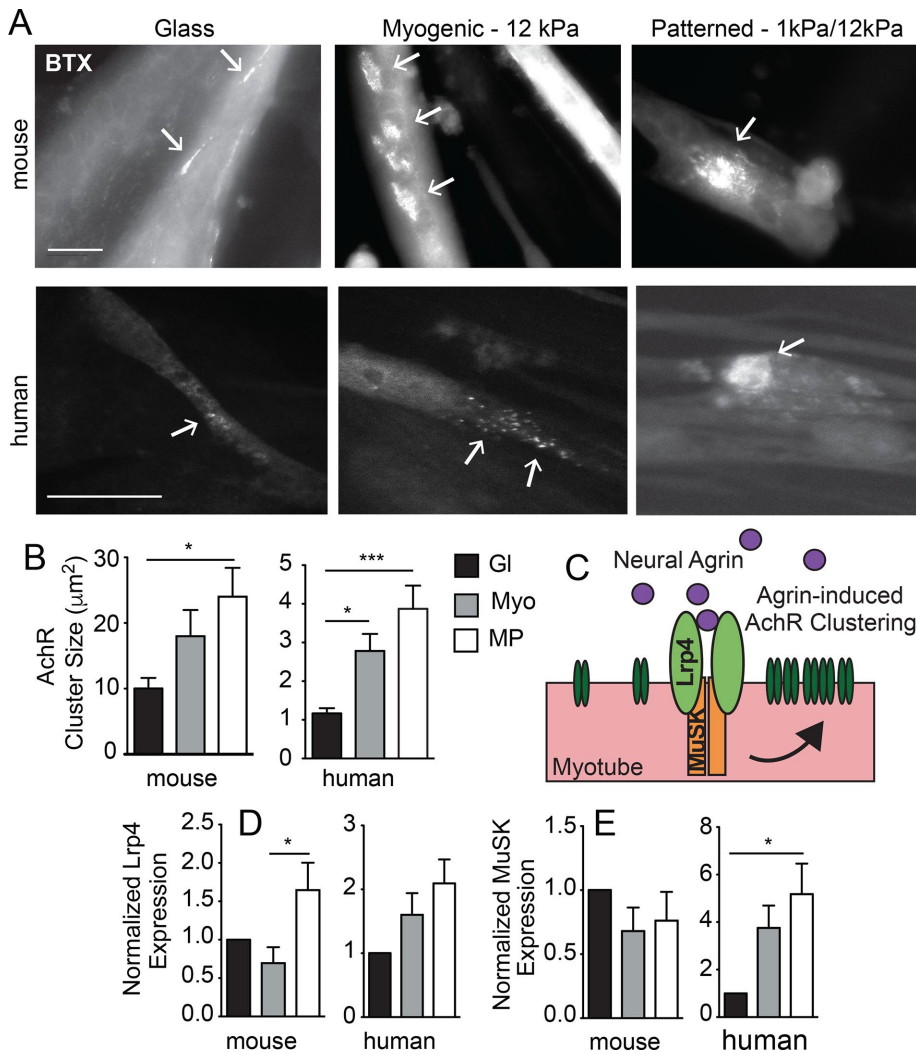


**FIGURE 4:** Patterning drives clustering of ACh receptors. (A) Representative fluorescence images of AChR clustering on agrin-treated myotubes cultured on glass, myogenic (Myo), or mechanically patterned (MP) hydrogels at 5 d (mouse) or 7 d (human) after induction of differentiation. AChRs were labeled with BTX. Scale bars, 25  $\mu\text{m}$ . (B) Average AChR cluster size for mouse (left;  $n = 5$ ) and human (right;  $n = 20$ ). (C) Agrin-driven AChR clustering involving Lrp4 and MuSK. (D) Lrp4 and (E) MuSK expression was assessed by qPCR, and data were normalized to transcript expression on glass and plotted for the indicated species ( $n = 6$ ).  $*p < 0.05$  and  $***p < 0.001$  based on ANOVA comparisons of the indicated groups.

expression levels of Lrp4 in myotubes grown on glass and unpatterned myogenic substrates may preclude their ability to respond to the improved agrin signaling that occurs in the coculture system.

To probe the role of substrate stiffness versus myotube alignment and fusion in the formation of AChR clusters, we differentiated mouse myotubes on patterned substrates of pathological stiffness. Cluster size was responsive to substrate stiffness, with smaller clusters expressed on pathological patterns, although there was no change in the extent of myotube fusion (Figure 7). These data suggest that AChR cluster size is regulated independently of myotube fusion, that is, clusters do not increase in size with increased myotube fusion, thus indicating a novel role for mechanotransduction in the control of AChR clustering. This pathway may be mediated by Wnt signaling, which is responsive to mechanical cues and involved in the Lrp4/MuSK signal cascade leading to AChR clustering (Henriquez and Salinas, 2012; Du *et al.*, 2016). Mechanosensitivity of the NMJ may have implications for MN or muscle diseases in which

muscle fibrosis occurs, such as ALS and Duchenne muscular dystrophy, and may contribute insight into the mechanisms of muscle denervation and atrophy (Klingler *et al.*, 2012; Carlson, 2014).

Although this system is relatively straightforward to assemble, several important caveats should be considered relative to existing systems. Most notably, we find that this system enables imaging for days in coculture, which is sufficient for nascent NMJs to form; beyond that time, our system exhibits similar delamination issues to other 2D technologies (Wang *et al.*, 2012), which could limit long-term utility with disease modeling. The 3D systems, despite complex fabrication, could provide long-term monitoring of patient-derived NMJs, although in vitro efforts in three dimensions have primarily focused on muscle (Sakar *et al.*, 2012; Cvetkovic *et al.*, 2014; Madden *et al.*, 2015; Bettadapur *et al.*, 2016; Raman *et al.*, 2016). A second consideration is the relative maturity of the junctions themselves; AChR clusters resemble more plaque-like morphology (Marques *et al.*, 2000; Huh and Fuhrer, 2002), and muscle twitch duration is long (Schiuffino and Reggiani, 2011; Umbach *et al.*, 2012), even when improved by mechanical patterning, suggesting formation of functional but fetal-like synapses and immature slow fiber-type muscles. Although only spontaneous contractions induced by MNs were examined here, improved optogenetic control could further tease out NMJ maturity by examining signal propagation across junctions. Indeed, optogenetic control of muscle in these types of systems has shown that human cells can be optically controlled to examine more complex behaviors in-a-dish (Sakar *et al.*, 2012; Raman *et al.*, 2016).

Despite these caveats, benefits specific to this NMJ-in-a-dish model are its relative ease of fabrication and the observation that mechanical patterning improves the maturation of hESC-derived skeletal muscle (Caron *et al.*, 2016). Other studies illustrated that human progenitors can be used to create functional NMJs (Demestre *et al.*, 2015; Puttonen *et al.*, 2015), but, to the best of our knowledge, this is the first demonstration that human myoblasts can be matured, fuse into patterned myotubes, and form functional NMJs in vitro. They appear to express more Lrp4 and MuSK and are more ACh sensitive than these other efforts, and so NMJs in these cells may represent a more mature state; however, side-by-side comparisons of these 2D methods is required to draw a better-supported conclusion. In addition, this system reveals that a mechanotransductive pathway that is not dependent on myotube fusion influences the formation of AChR clusters and may mediate the cellular response to pathological conditions, such as the fibrosis that occurs in muscle diseases. Thus we believe that this system represents the most straightforward and useful 2D NMJ-in-a-dish model for studying NMJ development and MN or muscle disease pathophysiology.

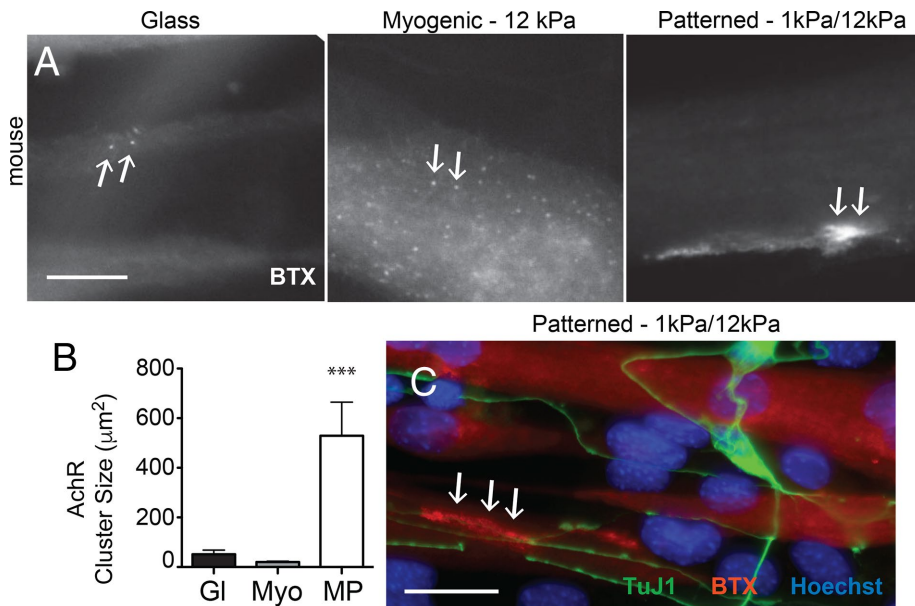


**FIGURE 5:** Patterning improves AChR clusters induced by MN coculture. (A) Representative fluorescence images of AChR clustering on mouse myotubes cocultured with mouse MN for 7 d. Myotubes were differentiated for 4 d before the start of the coculture. AChRs were labeled with BTX. Scale bar, 20  $\mu\text{m}$ . Arrows indicate BTX immunoreactivity. (B) Average AChR cluster size ( $n = 20$ ) for glass (Gl), soft myogenic substrates (Myo), and mechanically patterned hydrogels (MP). \*\*\* $p < 0.001$  based on ANOVA comparisons between substrate conditions. (C) Representative fluorescence image of patterned mouse myotube/mouse MN coculture at 7 d. Cells were immunostained with  $\beta$ -III-tubulin (TuJ1, green) and BTX (red) and counterstained for nuclei with Hoechst 33352 (blue). Scale bar, 30  $\mu\text{m}$ . Arrows indicate BTX immunoreactivity that colocalizes with  $\beta$ -III-tubulin immunoreactivity, suggestive of a putative NMJ.

## MATERIALS AND METHODS

### Mechanically patterned gel fabrication

Mechanically patterned hydrogels were fabricated using a two-step PA photopolymerization method (Figure 1A) modified from established methods (Marklein and Burdick, 2010; Tse and Engler, 2010) but that differs from them (Choi *et al.*, 2012b). First, single-modulus PA hydrogels were polymerized onto methacrylated 18-mm glass coverslips from a prepolymer solution containing acrylamide (3%), bis-acrylamide (0.4%), and 2-hydroxy-4'-(2-hydroxyethoxy)-2-methylpropiophenone (0.5%). The prepolymer solution was sandwiched between the methacrylated glass and a chlorosilanated glass slide and exposed to ultraviolet (UV) light (350 nm) for 5 min. After polymerization, the PA hydrogel was removed from the chlorosilanated glass slide, dehydrated overnight, and then rehydrated with a second prepolymer solution consisting of acrylamide (4% for myogenic mechanically patterned substrates and 4.5% for pathological mechanically patterned substrates), bis-acrylamide (0.4%), and 2-hydroxy-4'-(2-hydroxyethoxy)-2-methylpropiophenone (0.5%). The rehydrated PA gel was exposed to UV light (350 nm) for 5 min through a high-resolution chrome photomask patterned with alternating black (200- $\mu\text{m}$  width) and clear (100- $\mu\text{m}$  width) stripes. The resultant pattern on the PA hydrogel was softer, 200- $\mu\text{m}$ -wide stripes alternating with stiffer, 100- $\mu\text{m}$ -wide stripes. The bis-acrylamide concentration was maintained at a relatively high 0.4% (wt/vol) concentration to minimize the amount of differential swelling that might occur in adjacent stripes (Charest *et al.*, 2012; Choi *et al.*, 2012a).

To fabricate single-modulus myogenic PA hydrogels, a prepolymer solution consisting of acrylamide (6.25%), bis-acrylamide (0.4%), and 2-hydroxy-4'-(2-hydroxyethoxy)-2-methylpropiophenone (0.5%) was used. After polymerization, the hydrogels were washed thor-

oughly with phosphate-buffered saline (PBS) to remove any unreacted monomer or cross-linker and stored in PBS at 4°C.

The surfaces of the mechanically and myogenic hydrogels were functionalized with collagen IV using a photoactivating cross-linker, sulfosuccinimidyl 6-(4'-azido-2'-nitrophenylamino)hexanoate (Sulfo-SANPAH; Pierce). The hydrogels were immersed in 4-(2-hydroxyethyl)-1-piperazineethanesulfonic acid buffer (pH 8.4, 50 mM) containing Sulfo-SANPAH (0.2 mg/ml) and exposed to UV light (350 nm) for 10 min. After several washes in PBS, the hydrogels were incubated in collagen IV (100  $\mu\text{g}/\text{ml}$ ) overnight at 37°C.

### Mechanical characterization

Substrate stiffness was measured via indentation using an MFP-3D-Bio (Asylum Research, Santa Barbara, CA) atomic force microscope (AFM). We used chromium/gold-coated, silicon nitride (SiN) cantilevers with pyramidal tips (PNP-TR; NanoWorld) with a nominal spring constant of  $\sim 30$  pN/nm, as determined from the MFP-3Ds built-in thermal calibration function. Samples were mounted on glass slides using vacuum grease and immersed in PBS. The probe was indented into the sample with an approach velocity of 2  $\mu\text{m}/\text{s}$  and a force trigger of 2 nN. AFM data were analyzed using custom code in Igor Pro

(Wavemetrics); the substrate spring constant, that is, Young's modulus, was determined using a linearized Sneddon model (Kaushik *et al.*, 2011).

### Cell line and human embryonic stem cell-derived myotube culture

C2C12 mouse myoblast cell line, which was validated by the American Type Culture Collection (CRL-1772), was seeded on the surface of mechanically patterned and myogenic hydrogels or glass coverslips coated with collagen IV (100  $\mu\text{g}/\text{ml}$ ) at a density of 4000 cells/ $\text{cm}^2$  and maintained in growth medium consisting of DMEM (with 4.5 g/l glucose, with glutamine, without sodium pyruvate), fetal bovine serum (FBS; 20%), and penicillin/streptomycin (1%). After 2 d in growth medium, the cultures were switched to differentiation medium consisting of DMEM, horse serum (2%), insulin (2  $\mu\text{g}/\text{ml}$ ), and penicillin/streptomycin (1%). At 1 d after the onset of differentiation, cultures were treated with agrin (100 ng/ml) to induce AChR clustering, and at 2 d after the onset of differentiation, cultures were treated with cytosine  $\beta$ -D-arabinofuranoside (10  $\mu\text{M}$ ) to inhibit myoblast proliferation. At 5 d after the onset of differentiation, cultures were either assayed for functional activity or terminated for immunofluorescence and RNA analysis.

The hESC-derived myoblasts (GENEA002) were obtained and validated by Genea Biocells (La Jolla, CA) through prior publication (Caron *et al.*, 2016). Cells were seeded onto hydrogels or glass coverslips coated with collagen I (100  $\mu\text{g}/\text{ml}$ ) at a density of 15,000 cells/ $\text{cm}^2$  and maintained in growth medium (SKM-02; Genea Biocells) for 3 d. Cultures were then changed to differentiation medium (SKM-03; Genea Biocells) and maintained for 7 d before functional analysis or fixation for immunofluorescence and RNA analysis.

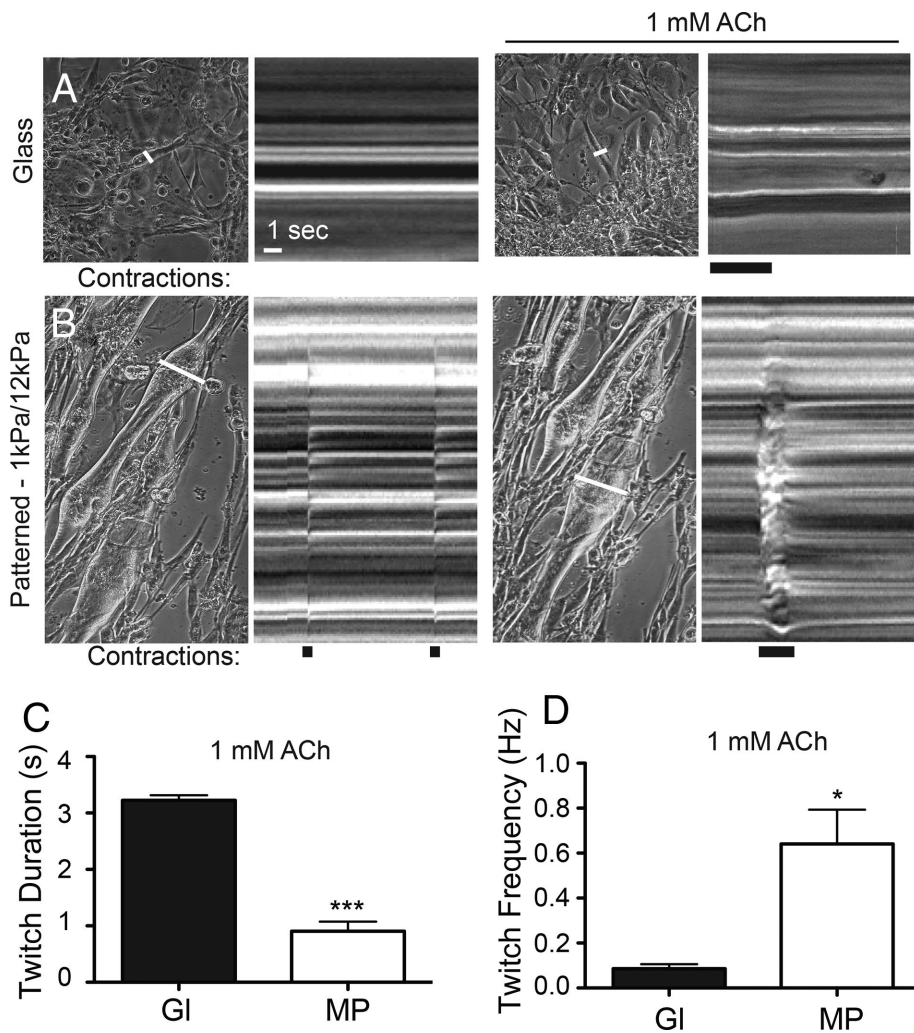


**FIGURE 6:** Functional assessment of AChR clusters in myotubes on different substrates. (A, B) Still movie images of myotube cultures (left). The white line indicates which contracting myotube was used to create the associated kymograph (right). The black bar at the bottom of each kymograph notes contractions. Cultures were stimulated with ACh as indicated. (C) Twitch duration and (D) frequency for glass (GI; black) and mechanically patterned hydrogels (MP; white;  $n = 5$ ). \* $p < 0.05$  and \*\*\* $p < 0.001$  based on ANOVA comparisons between substrate conditions.

### Isolation of rat primary MNs and their coculture with myotubes

The use of rats in this study was approved by UC San Diego's Institutional Animal Care and Use Committee review board (Protocol # S11032). Mouse embryonic motor neurons were isolated from the spinal cords of embryonic day 12 CD1 mouse embryos using a discontinuous density gradient centrifugation purification technique (Gingras *et al.*, 2007). Purified motor neurons were cocultured with established C2C12 myotube cultures at 4 d after the onset of myotube differentiation. The cocultures were maintained in motor neuron medium consisting of Neurobasal medium, B27 supplement (2%), glutamine (0.5 mM), hydrocortisone (400 ng/ml), insulin (2  $\mu$ g/ml), FBS (10%), and penicillin/streptomycin (1%).

### Immunofluorescence staining, fusion characterization, and AChR characterization

Cultures were fixed with 3.7% formaldehyde for 25 min at room temperature, permeabilized with 1% Triton-X for 5 min, and then

incubated in PBS containing 5% goat serum for 20 min at room temperature. Samples were incubated in primary antibodies at 4°C overnight, washed in PBS, and then incubated in secondary antibodies for 45 min at room temperature, followed by a 10-min incubation in Hoechst 33352 (1:1000 in PBS) to counterstain nuclei. Primary antibodies used in this study were hybridoma-derived anti-myosin heavy chain (1:50, MF20; Developmental Studies Hybridoma Bank) and rabbit polyclonal anti- $\beta$ -III-tubulin (1:500, ab18207; Abcam). Alexa Fluor 488 secondary antibody was used (1:1000; Fisher Scientific). To label AChR clusters, samples were incubated with  $\alpha$ -bungarotoxin (BTX) conjugated with Alexa Fluor 555 (1:500; Molecular Probes) for 45 min at room temperature.

Myoblast fusion index was calculated as the percentage of Hoechst-positive cell nuclei residing within MF20-positive myotubes. Average myotube width was calculated by measuring the width at the widest point on the myotube using the ImageJ measure function. For each metric, data were collected from 20 representative 20 $\times$  images. BTX-immunoreactivity on 5 (mouse) or 20 (human) representative 60 $\times$  images was used to evaluate AChR clustering. Average cluster size was quantified by manual tracing using ImageJ software. The width of each myotube that expressed AChR clusters was recorded and plotted against AChR cluster area to evaluate the correlation between cluster size and myotube width.

### Quantitative PCR

RNA was collected from cultures using TRIzol isolation, and cDNA was synthesized from 2  $\mu$ g of RNA using reverse transcriptase PCR (37°C for 60 min, 99°C for 5 min, and 5°C for 5 min) with Superscript II Reverse Transcriptase (Invitrogen) and 2.5 mM random hexamer mix (Invitrogen). Quantitative PCR (qPCR) was carried out using a CFX96 Real-Time PCR Detection system using iQ SYBR Green Supermix (2 min at 50°C followed by 10 min at 95°C for one cycle, then 15 s at 95°C followed by 1 min at 60°C for 40 cycles) and custom designed primers (Supplemental Table S1). Expression levels were calculated based on a standard curve generated by fibronectin plasmid. All data were normalized to glyceraldehyde-3-phosphate dehydrogenase (GAPDH), and data from the myogenic and MP hydrogels are presented as the fold change from the glass control.

### Functional assessment of myotubes

Bright-field video images were acquired with a CoolSnap HQ camera (Photometrics Scientific) through a Nikon Eclipse Ti inverted microscope with a 10 $\times$  objective.

Myotube monocultures were assessed for ACh responsiveness after 5 d in culture (mouse) or 7 d in culture (human). Videos were collected at 9.2 frames/s and captured before and immediately after

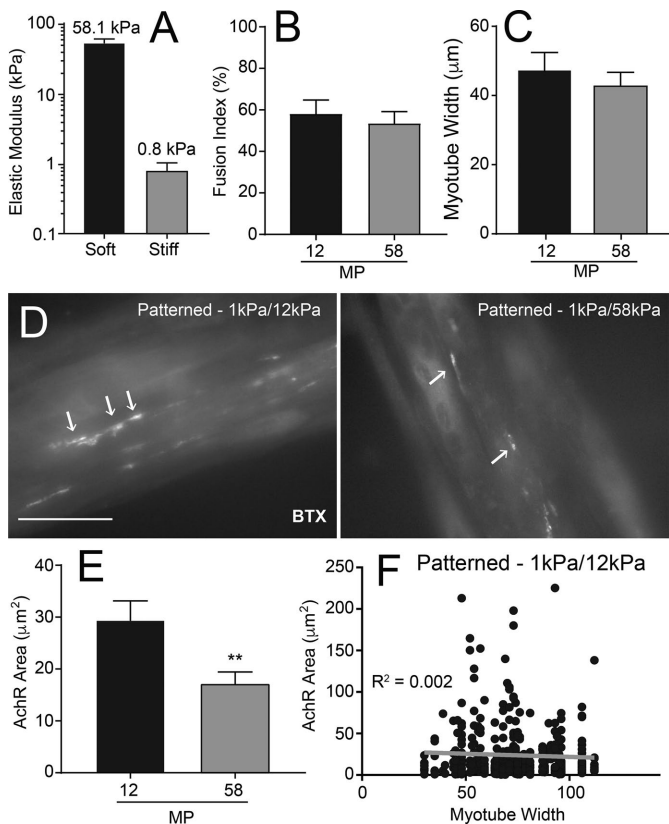


**FIGURE 7:** Substrate stiffness, but not myotube width, mediates AChR cluster formation on mechanically patterned substrates. (A) Elastic modulus of pathological mechanically patterned hydrogel. Fusion index (B) and myotube width (C) of mouse myotubes cultured on mechanically patterned hydrogels with myogenic (12 kPa) and pathological (58 kPa) stiff regions ( $n = 25$ ). (D) Representative fluorescence images of AChR clustering on patterned hydrogels. AChR clusters are labeled with BTX. Scale bar, 10  $\mu\text{m}$ . Arrows indicate AChR clusters. (E) AChR cluster area on myotubes cultured with agrin treatment on patterned hydrogels ( $n = 25$ ).  $**p < 0.01$  based on unpaired  $t$  test comparison. (F) Scatter plot of AChR cluster size vs. myotube width on mechanically patterned substrates with myogenic (12 kPa) stiff regions ( $n = 236$  AChR clusters).

stimulation with 1 mM ACh chloride (Sigma-Aldrich) in a 10- $\mu\text{l}$  volume. Kymographs of myotube contraction were generated using ImageJ software.

### Statistical analysis

All data are presented as the mean  $\pm$  SEM. Statistical analysis was carried out with GraphPad Prism software using one-way analysis of variance (ANOVA) tests, unpaired  $t$  test, or linear regression analysis, as appropriate. Statistical significance was considered at  $p < 0.05$ .

### ACKNOWLEDGMENTS

We thank Heather Main and Jamshid Arjomand (Genea Biocells) for use of hESC-derived myoblasts. We acknowledge funding support from the National Institutes of Health (DP2OD006460 to A.J.E. and F32HL131424 to C.L.H.) and the National Science Foundation (1463689 to A.J.E.), as well as support via the National Science Foundation Graduate Research Fellowship Program (to A.K.G.).

### REFERENCES

- Abujarour R, Valamehr B (2015). Generation of skeletal muscle cells from pluripotent stem cells: advances and challenges. *Front Cell Dev Biol* 3, 29.
- Altomare L, Riehle M, Gadegaard N, Tanzi MC, Fare S (2010). Microcontact printing of fibronectin on a biodegradable polymeric surface for skeletal muscle cell orientation. *Int J Artif Organs* 33, 535–543.
- Bettadapur A, Suh GC, Geisse NA, Wang ER, Hua C, Huber HA, Viscio AA, Kim JY, Strickland JB, McCain ML (2016). Prolonged culture of aligned skeletal myotubes on micromolded gelatin hydrogels. *Sci Rep* 6, 28855.
- Carlon BM (2014). The biology of long-term denervated skeletal muscle. *Eur J Transl Myol* 24, 3293.
- Caron L, Kher D, Lee KL, McKernan R, Dumevska B, Hidalgo A, Li J, Yang H, Main H, Ferri G, et al. (2016). A human pluripotent stem cell model of facioscapulohumeral muscular dystrophy-affected skeletal muscles. *Stem Cells Transl Med* 5, 1145–1161.
- Charest JM, Califano JP, Carey SP, Reinhart-King CA (2012). Fabrication of substrates with defined mechanical properties and topographical features for the study of cell migration. *Macromol Biosci* 12, 12–20.
- Chen CS, Mrksich M, Huang S, Whitesides GM, Ingber DE (1997). Geometric control of cell life and death. *Science* 276, 1425–1428.
- Chipman PH, Zhang Y, Rafuse VF (2014). A stem-cell based bioassay to critically assess the pathology of dysfunctional neuromuscular junctions. *PLoS One* 9, e91643.
- Choi YS, Vincent LG, Lee AR, Dobke MK, Engler AJ (2012a). Mechanical derivation of functional myotubes from adipose-derived stem cells. *Biomaterials* 33, 2482–2491.
- Choi YS, Vincent LG, Lee AR, Kretschmer KC, Chirasatitsin S, Dobke MK, Engler AJ (2012b). The alignment and fusion assembly of adipose-derived stem cells on mechanically patterned matrices. *Biomaterials* 33, 6943–6951.
- Cvetkovic C, Raman R, Chan V, Williams BJ, Tolish M, Bajaj P, Sakar MS, Asada HH, Saif MT, Bashir R (2014). Three-dimensionally printed biological machines powered by skeletal muscle. *Proc Natl Acad Sci USA* 111, 10125–10130.
- Das M, Rumsey JW, Bhargava N, Stancescu M, Hickman JJ (2010). A defined long-term in vitro tissue engineered model of neuromuscular junctions. *Biomaterials* 31, 4880–4888.
- Das M, Rumsey JW, Gregory CA, Bhargava N, Kang JF, Molnar P, Riedel L, Guo X, Hickman JJ (2007). Embryonic motoneuron-skeletal muscle coculture in a defined system. *Neuroscience* 146, 481–488.
- Demestre M, Orth M, Fohr KJ, Achberger K, Ludolph AC, Liebau S, Boeckers TM (2015). Formation and characterisation of neuromuscular junctions between hiPSC derived motoneurons and myotubes. *Stem Cell Res* 15, 328–336.
- Du J, Zu Y, Li J, Du S, Xu Y, Zhang L, Jiang L, Wang Z, Chien S, Yang C (2016). Extracellular matrix stiffness dictates Wnt expression through integrin pathway. *Sci Rep* 6, 20395.
- Engler AJ, Griffin MA, Sen S, Bonnemann CG, Sweeney HL, Discher DE (2004). Myotubes differentiate optimally on substrates with tissue-like stiffness: pathological implications for soft or stiff microenvironments. *J Cell Biol* 166, 877–887.
- Engler AJ, Sen S, Sweeney HL, Discher DE (2006). Matrix elasticity directs stem cell lineage specification. *Cell* 126, 677–689.
- Faravelli I, Frattini E, Ramirez A, Stuppia G, Nizzardo M, Corti S (2014). iPSC-based models to unravel key pathogenetic processes underlying motor neuron disease development. *J Clin Med* 3, 1124–1145.
- Gaudel C, Schwartz C, Giordano C, Abumrad NA, Grimaldi PA (2008). Pharmacological activation of PPARbeta promotes rapid and calcineurin-dependent fiber remodeling and angiogenesis in mouse skeletal muscle. *Am J Physiol Endocrinol Metab* 295, E297–E304.
- Gibbons MC, Sato EJ, Bachasson D, Cheng T, Azimi H, Schenk S, Engler AJ, Singh A, Ward SR (2016). Muscle architectural changes after massive human rotator cuff tear. *J Orthop Res* 34, 2089–2095.
- Gingras M, Gagnon V, Minotti S, Durham HD, Berthod F (2007). Optimized protocols for isolation of primary motor neurons, astrocytes and microglia from embryonic mouse spinal cord. *J Neurosci Methods* 163, 111–118.
- Guo X, Gonzalez M, Stancescu M, Vandenburgh HH, Hickman JJ (2011). Neuromuscular junction formation between human stem cell-derived motoneurons and human skeletal muscle in a defined system. *Biomaterials* 32, 9602–9611.
- Henriquez JP, Salinas PC (2012). Dual roles for Wnt signalling during the formation of the vertebrate neuromuscular junction. *Acta Physiol (Oxf)* 204, 128–136.

- Huh KH, Fuhrer C (2002). Clustering of nicotinic acetylcholine receptors: from the neuromuscular junction to interneuronal synapses. *Mol Neurobiol* 25, 79–112.
- Inoue H, Nagata N, Kurokawa H, Yamanaka S (2014). iPS cells: a game changer for future medicine. *EMBO J* 33, 409–417.
- Kaushik G, Fuhrmann A, Cammarato A, Engler AJ (2011). In situ mechanical analysis of myofibrillar perturbation and aging on soft, bilayered *Drosophila* myocardium. *J Biophys* 101, 2629–2637.
- Kim N, Stiegler AL, Cameron TO, Hallock PT, Gomez AM, Huang JH, Hubbard SR, Dustin ML, Burden SJ (2008). Lrp4 is a receptor for Agrin and forms a complex with MuSK. *Cell* 135, 334–342.
- Klingler W, Jurkat-Rott K, Lehmann-Horn F, Schleip R (2012). The role of fibrosis in Duchenne muscular dystrophy. *Acta Myol* 31, 184–195.
- Lawlor MW, Viola MG, Meng H, Edelstein RV, Liu F, Yan K, Luna EJ, Lerch-Gaggl A, Hoffmann RG, Pierson CR, et al. (2014). Differential muscle hypertrophy is associated with satellite cell numbers and Akt pathway activation following activin type IIB receptor inhibition in Mtm1 p.R69C mice. *Am J Pathol* 184, 1831–1842.
- Lenzi J, Pagani F, De Santis R, Limatola C, Bozzoni I, Di Angelantonio S, Rosa A (2016). Differentiation of control and ALS mutant human iPSCs into functional skeletal muscle cells, a tool for the study of neuromuscular diseases. *Stem Cell Res* 17, 140–147.
- Madden L, Juhas M, Kraus WE, Truskey GA, Bursac N (2015). Bioengineered human myobundles mimic clinical responses of skeletal muscle to drugs. *Elife* 4, e04885.
- Marklein RA, Burdick JA (2010). Spatially controlled hydrogel mechanics to modulate stem cell interactions. *Soft Matter* 6, 136–143.
- Marques MJ, Conchello JA, Lichtman JW (2000). From plaque to pretzel: fold formation and acetylcholine receptor loss at the developing neuromuscular junction. *J Neurosci* 20, 3663–3675.
- Morimoto Y, Kato-Negishi M, Onoe H, Takeuchi S (2013). Three-dimensional neuron-muscle constructs with neuromuscular junctions. *Biomaterials* 34, 9413–9419.
- Picher-Martel V, Valdmans PN, Gould PV, Julien JP, Dupre N (2016). From animal models to human disease: a genetic approach for personalized medicine in ALS. *Acta Neuropathol Commun* 4, 70.
- Pioro EP, Mitsumoto H (1995). Animal models of ALS. *Clin Neurosci* 3, 375–385.
- Puttonen KA, Ruponen M, Naumenko N, Hovatta OH, Tavi P, Koistinaho J (2015). Generation of functional neuromuscular junctions from human pluripotent stem cell lines. *Front Cell Neurosci* 9, 473.
- Raman R, Cvetkovic C, Uzel SG, Platt RJ, Sengupta P, Kamm RD, Bashir R (2016). Optogenetic skeletal muscle-powered adaptive biological machines. *Proc Natl Acad Sci USA* 113, 3497–3502.
- Sakar MS, Neal D, Boudou T, Borochin MA, Li Y, Weiss R, Kamm RD, Chen CS, Asada HH (2012). Formation and optogenetic control of engineered 3D skeletal muscle bioactuators. *Lab Chip* 12, 4976–4985.
- Schiaffino S, Reggiani C (2011). Fiber types in mammalian skeletal muscles. *Physiol Rev* 91, 1447–1531.
- Shi L, Fu AK, Ip NY (2012). Molecular mechanisms underlying maturation and maintenance of the vertebrate neuromuscular junction. *Trends Neurosci* 35, 441–453.
- Siller R, Greenhough S, Park IH, Sullivan GJ (2013). Modelling human disease with pluripotent stem cells. *Curr Gene Ther* 13, 99–110.
- Singhal N, Martin PT (2011). Role of extracellular matrix proteins and their receptors in the development of the vertebrate neuromuscular junction. *Dev Neurobiol* 71, 982–1005.
- Steinbeck JA, Jaiswal MK, Calder EL, Kishinevsky S, Weishaupt A, Toyka KV, Goldstein PA, Studer L (2016). Functional connectivity under optogenetic control allows modeling of human neuromuscular disease. *Cell Stem Cell* 18, 134–143.
- Tay A, Schweizer FE, Di Carlo D (2016). Micro- and nano-technologies to probe the mechano-biology of the brain. *Lab Chip* 16, 1962–1977.
- Tse JR, Engler AJ (2010). Preparation of hydrogel substrates with tunable mechanical properties. *Curr Protoc Cell Biol* Chapter 10, Unit 10.16.
- Umbach JA, Adams KL, Gundersen CB, Novitsch BG (2012). Functional neuromuscular junctions formed by embryonic stem cell-derived motor neurons. *PLoS One* 7, e36049.
- Uzel SG, Platt RJ, Subramanian V, Pearl TM, Rowlands CJ, Chan V, Boyer LA, So PT, Kamm RD (2016). Microfluidic device for the formation of optically excitable, three-dimensional, compartmentalized motor units. *Sci Adv* 2, e1501429.
- Vincent LG, Choi YS, Alonso-Latorre B, del Alamo JC, Engler AJ (2013). Mesenchymal stem cell durotaxis depends on substrate stiffness gradient strength. *Biotechnol J* 8, 472–484.
- Viollet L, Melki J (2013). Spinal muscular atrophies. *Handb Clin Neurol* 113, 1395–1411.
- Wang PY, Thissen H, Tsai WB (2012). The roles of RGD and grooved topography in the adhesion, morphology, differentiation of C2C12 skeletal myoblasts. *Biotechnol Bioeng* 109, 2104–2115.
- Wen JH, Choi O, Taylor-Weiner H, Fuhrmann A, Karpiak JV, Almutairi A, Engler AJ (2015). Haptotaxis is cell type specific and limited by substrate adhesiveness. *Cell Mol Bioeng* 8, 530–542.
- Wijesekera LC, Leigh PN (2009). Amyotrophic lateral sclerosis. *Orphanet J Rare Dis* 4, 3.
- Witzemann V (2006). Development of the neuromuscular junction. *Cell Tissue Res* 326, 263–271.
- Wu H, Xiong WC, Mei L (2010). To build a synapse: signaling pathways in neuromuscular junction assembly. *Development* 137, 1017–1033.
- Zhang B, Luo S, Wang Q, Suzuki T, Xiong WC, Mei L (2008). LRP4 serves as a coreceptor of agrin. *Neuron* 60, 285–297.
- Zhu J, Li Y, Lu A, Gharaibeh B, Ma J, Kobayashi T, Quintero AJ, Huard J (2011). Follistatin improves skeletal muscle healing after injury and disease through an interaction with muscle regeneration, angiogenesis, and fibrosis. *Am J Pathol* 179, 915–930.